J Math Chem (2012) 50:765–781
DOI 10.1007/s10910-011-9923-3

ORIGINAL PAPER

Automatic simulation of electrochemical transients by the adaptive Huber method for Volterra integral equations involving Kernel terms $\exp[-\alpha(t-\tau)]\mathrm{erex}\{[\beta(t-\tau)]^{1/2}\}$ and $\exp[-\alpha(t-\tau)]\mathrm{daw}\{[\beta(t-\tau)]^{1/2}\}$

Lesław K. Bieniasz

Received: 6 July 2011 / Accepted: 27 September 2011 / Published online: 8 October 2011

Abstract Development of fully automatic methods for the simulation of transient experiments in electroanalytical chemistry is a desirable element of the contemporary trends of laboratory automation in electrochemistry. In accord with this idea, the adaptive Huber method, elaborated by the present author, is intended to solve automatically integral equations of Volterra type, encountered in the theory of controlled-potential transients. The coefficients of the method have been recently obtained for integral transformation kernels involving terms $K(t,\tau) = \exp[-\alpha(t-\tau)]\mathrm{erex}\{[\beta(t-\tau)]^{1/2}\}$ and $K(t,\tau) = \exp[-\alpha(t-\tau)]\mathrm{daw}\{[\beta(t-\tau)]^{1/2}\}$ with $\alpha \geq 0$ and $\beta \geq 0$, which are known to occur in the above integral equations. In this work the validity of the resulting method, for electrochemical simulations, is examined using representative examples of electroanalytical models involving integral equations with various special cases of such kernel terms. The performance of the method is found similar to that previously reported for integral equations involving exclusively kernels $K(t,\tau) = 1$, $K(t,\tau) = (t-\tau)^{-1/2}$, and $K(t,\tau) = \exp[-\lambda(t-\tau)](t-\tau)^{-1/2}$ with $\lambda > 0$.

Keywords Computational electrochemistry · Laboratory automation · Voltammetry · Digital simulation · Volterra integral equations · Weakly singular kernels

L. K. Bieniasz (✉)
Department of Complex Systems and Chemical Processing of Information, Institute of Physical Chemistry of the Polish Academy of Sciences, ul. Niezapominajek 8, 30-239 Cracow, Poland
e-mail: nbbienia@cyf-kr.edu.pl
URL: http://www.cyf-kr.edu.pl/∼nbbienia

L. K. Bieniasz
Faculty of Physics, Mathematics, and Computer Science, Cracow University of Technology, ul. Warszawska 24, 31-155 Cracow, Poland

1 Introduction

In the present work we continue the long-term research program [1] aimed at supplying the electrochemical community with a comprehensive collection of automatic digital simulation methods [2] and problem solving environments [3,4] for the modelling of electrochemical transient experiments [5]. The intention of the program is to extend the contemporary ideas of laboratory automation in electroanalytical chemistry [6–8] onto modelling activities [9]. Specifically, we continue the development and testing of the adaptive variant of the Huber method [10] for solving electrochemical Volterra integral equations (IEs), recently described by the present author [11–18]. The method is the first simulation technique ever designed to solve the electrochemical kinetic IEs automatically, in the sense that numerical solutions can be obtained with a prescribed accuracy, without prior knowledge of their temporal behaviour and corresponding optimum discrete time grids needed for calculations. The method was initially formulated for single Abel IEs [11–13], then it was extended to single second kind Volterra IEs with non-linear dependencies on the unknown functions and their integrals [14,15], and later it was also generalised to systems of such IEs [16,17]. The integrals occurring in the IEs are assumed to take the form

$$Y(t) \;=\; \int_0^t K(t,\;\tau)\;\chi(\tau)\;d\tau \tag{1}$$

where $Y(t)$ denotes the integral, $K(t,\tau)$ is one of the possible integral transformation kernels, and $\chi(t)$ is one of the unknown functions. Most frequently these are cyclic voltammetric current functions, so that we use here the traditional symbol χ to denote the unknowns, although the method is not limited to cyclic voltammetry. In Refs. [10–17] the theoretical development and testing of the method was concentrated on three kernels most often encountered in electrochemistry: $K(t,\tau) = 1$, $K(t,\tau) = (t-\tau)^{-1/2}$, and $K(t,\tau) = \exp[-\lambda(t-\tau)](t-\tau)^{-1/2}$ with $\lambda > 0$. However, there are also electrochemical IEs involving other kernel functions, and if the method is to be comprehensive, it has to be extended to such other kernels. The extension consists in deriving a set of kernel-specific coefficients, which are used by the method for computing the discrete values of the current functions $\chi(t)$ and their error estimates. Ideally, the coefficients should be derived analytically for every new kernel function, because this ensures the best performance of the method, but sometimes this is not possible, and one has to resort to highly accurate numerical approximations to the coefficients.

The present work is devoted to the extension of the method onto IEs involving kernel terms:

$$K(t,\tau) = \exp[-\alpha(t-\tau)]\mathrm{erex}\{[\beta(t-\tau)]^{1/2}\} \tag{2}$$

and

$$K(t,\tau) = \exp[-\alpha(t-\tau)]\mathrm{daw}\{[\beta(t-\tau)]^{1/2}\} \tag{3}$$

In Eqs. (2) and (3) $\alpha \geq 0$ and $\beta \geq 0$ are constant parameters, $\mathrm{erex}(z) = \exp(z^2)\,\mathrm{erfc}(z)$, $\mathrm{erfc}(z) = 1 - \mathrm{erf}(z)$, with $\mathrm{erf}(z)$ denoting the error function $\mathrm{erf}(z) = 2\pi^{-1/2} \int_0^z \exp(-\zeta^2) d\zeta$, and $\mathrm{daw}(z)$ denoting the Dawson integral $\mathrm{daw}(z) = \exp(-z^2) \int_0^z \exp(\zeta^2) d\zeta$. Symbols α and β in Eqs. (2) and (3) should not be confused with the symbols of charge transfer coefficients or symmetry factors, frequently occurring in electrochemistry. Case $\alpha = \beta = 0$ of kernel (2) is equivalent to $K(t, \tau) = 1$, and has already been considered [14–17]. Case $\beta = 0$ of kernel (3) is equivalent to $K(t, \tau) = 0$ and is uninteresting. Depending on other possible combinations of the values of the parameters α and β, the following special cases A–F of the kernels (2) and (3) arise.

(A) for $\alpha > 0$ and $\beta = 0$ in (2):

$$K(t, \tau) = \exp\left[-\alpha(t - \tau)\right], \tag{4}$$

(B) for $\alpha = 0$ and $\beta > 0$ in (2):

$$K(t, \tau) = \mathrm{erex}\{[\beta\,(t - \tau)]^{1/2}\}, \tag{5}$$

(C) for $\alpha = \beta > 0$ in (2):

$$K(t, \tau) = \mathrm{erfc}\{[\beta\,(t - \tau)]^{1/2}\}, \tag{6}$$

(D) for $\alpha > 0$ and $\beta > 0, \alpha \neq \beta$ in (2):

$$K(t, \tau) = \exp[-\alpha(t - \tau)]\mathrm{erex}\{[\beta(t - \tau)]^{1/2}\}, \tag{7}$$

(E) for $\alpha = 0$ and $\beta > 0$ in (3):

$$K(t, \tau) = \mathrm{daw}\{[\beta\,(t - \tau)]^{1/2}\}, \tag{8}$$

(F) for $\alpha > 0$ and $\beta > 0$ in (3):

$$K(t, \tau) = \exp[-\alpha(t - \tau)]\mathrm{daw}\{[\beta(t - \tau)]^{1/2}\}. \tag{9}$$

There exist no single sets of formulae for the kernel-dependent coefficients of the adaptive Huber method, valid generally for kernels (2) and (3). Instead, every case A–F requires a separate set of formulae for the method coefficients. The derivations are tedious and prone to errors, and the final formulae are rather complicated. Approximations by series expansions are also necessary. Therefore, in order to avoid excessive technical descriptions here, all the derivations have been presented in detail in a separate paper [18], together with a set of non-electrochemical, but mathematically adequate tests verifying the correctness of the coefficients. Readers willing to write their own codes should consult Ref. [18], as well as the former papers about the method [11–17]. The purpose of the present paper is to demonstrate and document the performance of the adaptive Huber method, when the method is applied to representative examples of the IEs describing electrochemical transient experiments and containing various cases of kernel terms (2) and (3).

2 Examples

Cases A, B, D, E and F of kernels (2) and (3) have been encountered explicitly in electrochemical IEs of various physicochemical origin. In particular, case A occurs in the models of voltammetry for surface reaction mechanisms [19,20], when the models are formulated in terms of the IEs rather than ordinary differential equations. Case A occurs also in the modelling of voltammetry for spherical amalgam electrodes [21], tubular electrodes [22,23], and cylindrical pore electrodes [24,25]; in such situations the kernels are actually (theoretically infinite) sums involving exponential terms (4). Case B is the most characteristic of the IEs describing controlled-potential methods under conditions of diffusion to spherical electrodes [26–31]. However, it occurs also in the modelling of voltammetry for adsorption/diffusion electrochemistry at planar electrodes [32]. Case D has been reported for voltammetry and homogeneous catalytic mechanism at planar electrodes, when diffusion coefficients are unequal [33,34]. It also occurs for some homogeneous reaction-diffusion systems with equal diffusion coefficients, but in spherical geometry [35,36]. Finally, cases E and F have been obtained for voltammetry and homogeneous catalytic mechanism at planar electrodes, assuming unequal diffusion coefficients [33,34].

In Sect. 2.1–2.4 we describe four specific examples selected for the calculations.

2.1 Example 1: cyclic voltammetry for a surface ECE mechanism

As a testing example for the kernel case A, we choose a modification of the model of square-wave voltammetry for the surface ECE mechanism, described by Gulaboski [20]. The modification consists in replacing the square-wave perturbation by a cyclic voltammetric perturbation. The reaction mechanism: $\mathrm{A_{ad}} + n_1\mathrm{e}^- \rightleftharpoons \mathrm{B_{ad}}, \mathrm{B_{ad}} \rightarrow \mathrm{C_{ad}}, \mathrm{C_{ad}} + n_2\mathrm{e}^- \rightleftharpoons \mathrm{D_{ad}}$, involves two quasi-reversible charge transfer steps subject to Butler-Volmer kinetics, and one irreversible chemical reaction, between species $\mathrm{A}_{ad}, \mathrm{B}_{ad}, \mathrm{C}_{ad}$ and D_{ad} adsorbed at the electrode surface. Let us denote by $\theta_\mathrm{A}(t), \theta_\mathrm{B}(t), \theta_\mathrm{C}(t)$ and $\theta_\mathrm{D}(t)$ the surface concentrations of these species, normalised by the initial surface concentration Γ^* of $\mathrm{A_{ad}}$. Ordinary differential equations (2)–(5) in Ref. [20] can be expressed in the dimensionless form as:

$$d\theta_\mathrm{A}(t)/dt = -\psi_1(t) \tag{10}$$

$$d\theta_\mathrm{B}(t)/dt = \psi_1(t) - \lambda\theta_\mathrm{B}(t) \tag{11}$$

$$d\theta_\mathrm{C}(t)/dt = -\psi_2(t) + \lambda\theta_\mathrm{B}(t) \tag{12}$$

$$d\theta_\mathrm{D}(t)/dt = \psi_2(t) \tag{13}$$

where

$$\psi_1(t) = \kappa_1^0\left[\theta_\mathrm{A}(t)\, f_{c,1}(t) - \theta_\mathrm{B}(t)\, f_{a,1}(t)\right] \tag{14}$$

$$\psi_2(t) = \kappa_2^0\left[\theta_\mathrm{C}(t)\, f_{c,2}(t) - \theta_\mathrm{D}(t)\, f_{a,2}(t)\right] \tag{15}$$

with cathodic and anodic exponential terms

$$f_{c,i}(t) = \exp\{-\alpha_i n_i [u_i - S(t, t_s)]\} \quad (16)$$

$$f_{a,i}(t) = \exp\{(1-\alpha_i) n_i [u_i - S(t, t_s)]\} \quad (17)$$

for $i = 1, 2$. Symbols $\psi_i(t)$ denote dimensionless current functions, defined as current densities of the charge transfer steps, normalised by $n_i F^2 \Gamma^* v (RT)^{-1}$, where v is the rate of potential sweep, and F, R and T have the usual meaning. Symbols κ_i^0 for i =1, 2 denote conditional rate constants of the charge transfer steps, normalised by $Fv(RT)^{-1}$, corresponding cathodic charge transfer coefficients are denoted by α_i, and λ is the rate constant of the chemical reaction, normalised by $Fv(RT)^{-1}$. Symbols u_i denote dimensionless starting potential parameters, defined as $u_i = F(RT)^{-1}\left(E_{\text{start}} - E_i^0\right)$, where E_{start} is the starting potential and E_i^0 are formal potentials of the charge transfer steps. Dimensionless switching time $t_s = F(RT)^{-1}(E_{\text{start}} - E_{\text{switch}})$, where E_{switch} is the switching potential. Dimensionless time t is obtained by multiplying dimensional time by $Fv(RT)^{-1}$. $S(y, y_s)$ is the saw-tooth function:

$$S(y, y_s) = \begin{cases} y & \text{for } y \le y_s \\ 2y_s - y & \text{for } y > y_s \end{cases} \quad (18)$$

Equations (10)–(13) are accompanied by the initial conditions

$$\theta_{\text{A}}(0) = 1 \quad (19)$$

$$\theta_{\text{B}}(0) = \theta_{\text{C}}(0) = \theta_{\text{D}}(0) = 0 \quad (20)$$

By following the ideas from Ref. [20], the initial value problem (10)–(13), (19) and (20) can be expressed as an IE system for the unknown current functions $\psi_i(t)$:

$$\kappa_1^0 \left\{ f_{c,1}(t) \left[1 - \int_0^t \psi_1(\tau)\, d\tau \right] - f_{a,1}(t) \int_0^t \psi_1(\tau) \exp[-\lambda(t-\tau)]\, d\tau \right\} - \psi_1(t) = 0 \quad (21)$$

$$\kappa_2^0 \left\langle f_{c,2}(t) \left\{ \int_0^t \psi_1(\tau)\, d\tau - \int_0^t \psi_1(\tau) \exp[-\lambda(t-\tau)]\, d\tau - \int_0^t \psi_2(\tau)\, d\tau \right\} - f_{a,2}(t) \int_0^t \psi_2(\tau)\, d\tau \right\rangle - \psi_2(t) = 0 \quad (22)$$

2.2 Example 2: potential step chronoamperometry for an irreversible charge transfer at a spherical electrode

As a testing example for kernel case B it is particularly useful to consider potential step chronoamperometry for an irreversible transfer of n electrons at spherical electrodes, because analytical expression for the current is available [37], which allows

us to verify the correctness of the numerical solution. The relationship between the concentration $c(r_0, t)$, of a reactant at the surface of a spherical electrode with radius r_0, and the flux $f(r_0, t) = \partial c(r, t)/\partial r\,|_{r=r_0} = j(t)/(nF)$ related to the electric current density $j(t)$ is [26–31]:

$$c(r_0, t) = c^0 - D^{-1/2} \int_0^t \left\{ [\pi\,(t-\tau)]^{-1/2} - \rho\ \mathrm{erex}\left[\rho(t-\tau)^{1/2}\right] \right\} f\,(r_0, \tau)\ d\tau \tag{23}$$

where c^0 is the initial/bulk concentration, $\rho = D^{1/2}/r_0$, and D is the diffusion coefficient of the reactant. For the irreversible charge transfer

$$j(t)/(nF) = k\ c(r_0, t) \tag{24}$$

where k is a (potential-dependent) rate constant, which does not vary with time in a chronoamperometric experiment. We normalise time t by the duration t_{step} of the experiment, i.e. we substitute $t \leftarrow t/t_{\mathrm{step}}$. We also replace $\rho \leftarrow \rho\ t_{\mathrm{step}}^{1/2}$. By combining Eqs. (23) and (24), we then obtain the IE

$$\kappa \left\{ 1 - \int_0^t [\pi(t-\tau)]^{-1/2}\ \psi(\tau)\ d\tau + \rho \int_0^t \mathrm{erex}\left[\rho(t-\tau)^{1/2}\right]\ \psi(\tau)\ d\tau \right\} - \psi(t) = 0 \tag{25}$$

where $\kappa = k(D/t_{\mathrm{step}})^{-1/2}$ and $\psi(t) = j(t)/\left[nFc^0\left(D/t_{\mathrm{step}}\right)^{1/2}\right]$ is an unknown function to be determined. Using the same notation, the analytical expression [37] for $\psi(t)$ can be written as

$$\psi(t) = \frac{\kappa}{1+\kappa/\rho} \left\{ 1 + \frac{\kappa}{\rho} \mathrm{erex}\left[(\kappa + \rho)\, t^{1/2}\right] \right\}. \tag{26}$$

Equation (26) was derived in Ref. [37] by the Laplace transform method, without using the above IE formulation.

2.3 Example 3: cyclic voltammetry for an irreversible charge transfer at a spherical electrode

Another opportunity for testing the method on the kernel case B is offered by the theory of linear potential sweep voltammetry for an irreversible charge transfer subject to Butler-Volmer kinetics, at spherical electrodes. Such a theory was originally obtained by De Mars and Shain [38] with the help of finite-difference simulations. However, years later, Diao and Zhang [31] presented the IE pertinent to cyclic voltammetry for a quasi-reversible charge transfer at hemispherical microelectrodes. The IE for the

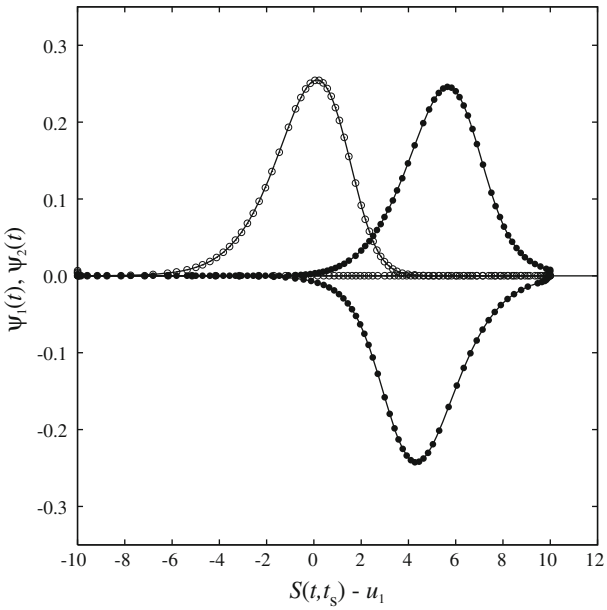

Fig. 1 Cyclic voltammetric current functions corresponding to $\kappa_1^0 = \kappa_2^0 = 1, \alpha_1 = \alpha_2 = 0.5, n_1 = n_2 = 1, \lambda = 1, u_1 = 10, u_2 = 15$, and $t_s = 20$, in example 1. The circles (*filled circle* and *open circle*) denote discrete values of the current functions $\psi_1(t)$ and $\psi_2(t)$, respectively, obtained by the adaptive Huber method from Eqs. (21) and (22), at the nodes of the temporal grid, assuming method parameters $tol = 10^{-4}$, $h_{\text{start}} = 0.01$ and $h_{max} = 1$. *Solid lines* represent reference solutions obtained by the DASSL integrator

irreversible reduction of n electrons can be obtained as a special case of the IE (27) from Ref. [31], or derived independently based on Eq. (23), with the result:

$$\int_0^t (t-\tau)^{-1/2}\,\chi(\tau)\,d\tau \;-\; \pi^{1/2}\rho \int_0^t \operatorname{erex}\left[\rho(t-\tau)^{1/2}\right] \chi(\tau)\,d\tau \;+\; \exp\left[u - S(t,t_s)\right]\,\chi(t) \;-\; 1 = 0 \tag{27}$$

where $\chi(t)$ is the dimensionless current function, defined in the standard way [39], t is the time normalised by $RT(\alpha_c n F v)^{-1}$, often denoted by bt in the literature, α_c is the cathodic charge transfer coefficient, $\rho = D^{1/2}[\alpha_c n F v (RT)^{-1}]^{-1/2}/r_0$, r_0 is the electrode radius, and D is the diffusion coefficient of the reactant. Parameter u equals $u = \alpha_c\, nF(RT)^{-1}\left(E_{\text{start}} - E^0\right) - \ln\left(k^0\right)$, where E_{start} is the starting potential, and E^0 and k^0 are the formal potential and conditional rate constant of the charge transfer reaction. Finally, $t_s = \alpha_c n F (RT)^{-1}(E_{\text{start}} - E_{\text{switch}})$, where E_{switch} is the switching potential.

For large ρ values (corresponding to small electrode radii) the voltammograms approach steady-state sigmoidal curves that can be derived from Eq. (27) in the way analogous to that described in the Appendix A in Ref. [40]:

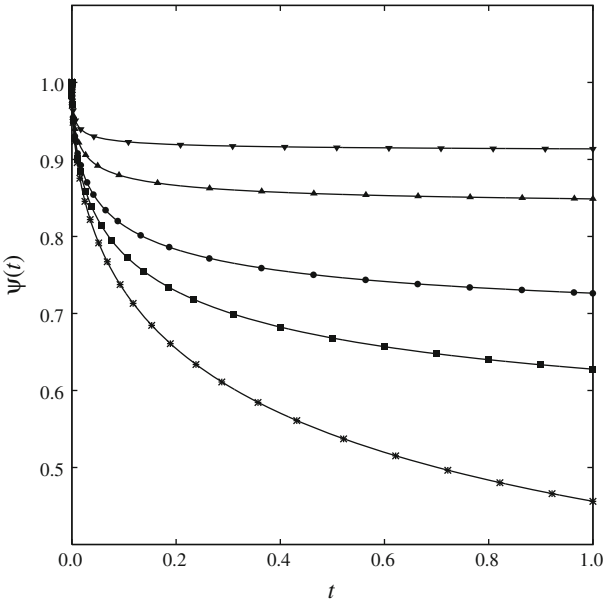

Fig. 2 Dimensionless chronoamperometric currents $\psi(t)$ obtained by the adaptive Huber method from Eq. (25), assuming $\kappa = 1$ and $\rho = 0.1$ (*asterisk*), 1 (*square*), 2 (*circle*), 5 (*triangle*) and 10 (*inverted triangle*) in example 2. Method parameters are: $tol = 10^{-4}$, $h_{\text{start}} = 10^{-10}$ and $h_{\max} = 0.1$. *Solid lines* represent analytical predictions of Eq. (26)

$$\chi(t) = \rho\pi^{-1/2}\left\{1 + \rho\pi^{-1/2}\exp\left[u - S(t, t_s)\right]\right\}^{-1} \tag{28}$$

By following the approach of Reinmuth [41], it is also possible to obtain the following exponential series solution of Eq. (27), valid for the forward potential sweep only:

$$\chi(t) = \sum_{j=1}^{\infty} b_j \exp\left[-j\,(u - t)\right] \tag{29}$$

where

$$b_j = \begin{cases} 1 & \text{for } j = 1 \\ (-1)^{j-1}\,\pi^{(j-1)/2} \Big/ \prod_{i=1}^{j-1}\left(\rho + i^{1/2}\right) & \text{for } j > 1 \end{cases} \tag{30}$$

2.4 Example 4: cyclic voltammetry for the catalytic mechanism at a planar electrode

In order to test the method on kernel cases D, E and F, we choose IEs from Ref. [34], describing cyclic voltammetry for the catalytic mechanism involving irreversible charge transfer and irreversible homogeneous reaction, under assumption of different diffusion coefficients, and for planar electrodes. Let us retain the notation from Ref. [34], according to which λ is the dimensionless rate constant of the homogeneous reaction, and δ is the ratio of diffusion coefficients. The IEs are:

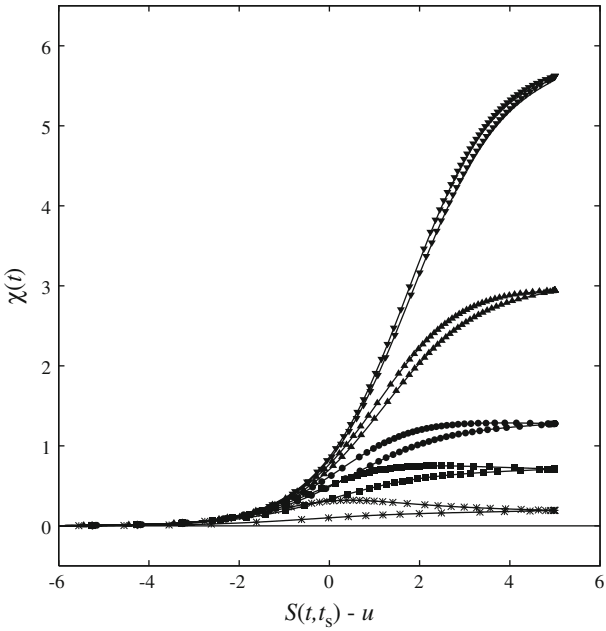

Fig. 3 Cyclic voltammetric current functions $\chi(t)$ obtained by the adaptive Huber method from Eq. (27), assuming $u = 15$, $t_s = 20$, and $\rho = 0.1$ (*asterisk*), 1 (*square*),2 (*circle*), 5 (*triangle*) and 10 (*inverted triangle*) in example 3. Method parameters are: $tol = 10^{-4}$, $h_{\text{start}} = 0.01$ and $h_{\max} = 1$. *Solid lines* represent reference solutions obtained by the Crank-Nicolson method. Initial parts of the voltammograms (where $\chi(t) \approx 0$) are not shown

$$\int_0^t (t-\tau)^{-1/2}\,\chi(\tau)\,d\tau \;+\; \left(\frac{\pi\lambda\delta}{1-\delta}\right)^{1/2}\left\{\int_0^t \exp[-\lambda(t-\tau)]\right.$$
$$\operatorname{erex}\left[\left(\frac{\lambda}{1-\delta}\right)^{1/2}(t-\tau)^{1/2}\right]\chi(\tau)\,d\tau$$
$$\left.-\int_0^t \operatorname{erex}\left[\left(\frac{\lambda\delta}{1-\delta}\right)^{1/2}(t-\tau)^{1/2}\right]\chi(\tau)\,d\tau\right\}$$
$$+\;\exp[u-S(t,t_s)]\,\chi(t)\;-\;1=\;0 \tag{31}$$

for $\delta < 1$, and

$$\int_0^t (t-\tau)^{-1/2}\,\chi(\tau)\,d\tau \;+\; 2\left(\frac{\lambda\delta}{\delta-1}\right)^{1/2}\left\{\int_0^t \exp[-\lambda(t-\tau)]\right.$$
$$\operatorname{daw}\left[\left(\frac{\lambda}{\delta-1}\right)^{1/2}(t-\tau)^{1/2}\right]\chi(\tau)\,d\tau$$

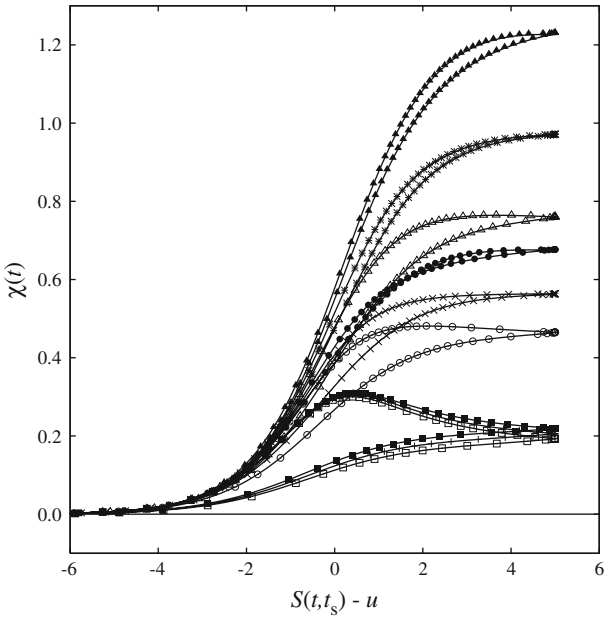

Fig. 4 Cyclic voltammetric current functions $\chi(t)$ obtained by the adaptive Huber method from Eqs.(31)–(33), assuming $u = 15$, $t_s = 20$, and $(\lambda, \delta) = (0.1, 1)$ (*plus sign*); $(1, 1)$(*multiplication sign*); $(3, 1)$(*asterisk*); $(0.1, 0.5)$ (*open square*); $(1, 0.5)$ (*open circle*); $(3, 0.5)$ (*open triangle*); $(0.1, 2)$ (*filled square*); $(1, 2)$ (*filled circle*); and $(3, 2)$ (*filled triangle*) in example 4. Method parameters are: $tol = 10^{-4}$, $h_{\text{start}} = 0.01$ and $h_{\max} = 1$. *Solid lines* represent reference solutions obtained by the Crank-Nicolson method. Initial parts of the voltammograms (where $\chi(t) \approx 0$) are not shown

$$-\int_0^t \text{daw}\left[\left(\frac{\lambda\delta}{\delta-1}\right)^{1/2}(t-\tau)^{1/2}\right]\chi(\tau)\,d\tau\Bigg\}$$
$$+\exp[u - S(t,t_s)]\,\chi(t) - 1 = 0 \tag{32}$$

for $\delta > 1$. Parameters u and t_s have the same meaning as in example 3. In the limit $\delta \to 1$ both Eqs.(31) and (32) converge to the IE:

$$\int_0^t \exp[-\lambda(t-\tau)](t-\tau)^{-1/2}\,\chi(\tau)\,d\tau + \exp[u - S(t,t_s)]\,\chi(t) - 1 = 0 \tag{33}$$

The adaptive solution of the IEs involving kernel $K(t,\tau) = \exp[-\lambda(t-\tau)](t-\tau)^{-1/2}$ occurring in Eq.(33) has been already discussed [14,15].

For large λ the voltammograms approach steady-state waves given by the formula [34]:

$$\chi(t) = \left(\lambda\delta\pi^{-1}\right)^{1/2}\left\{1 + \left(\lambda\delta\pi^{-1}\right)^{1/2}\exp[u - S(t,t_s)]\right\}^{-1} \tag{34}$$

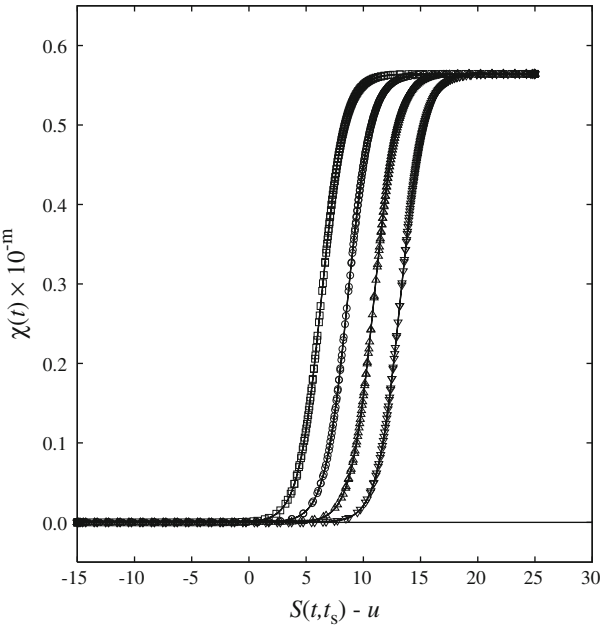

Fig. 5 Cyclic voltammetric current function $\chi(t)$ obtained by the adaptive Huber method from Eq. (27), assuming $u = 15, t_s = 40$, and $\rho = 10^m$, where m = 3 (*square*), 4 (*circle*), 5 (*triangle*) and 6 (*inverted triangle*) in example 3. Method parameters are: $tol = 10^{-4}$, $h_{\text{start}} = 0.01$ and $h_{\max} = 1$. *Solid lines* represent analytical steady-state current functions given by Eq. (28)

Series solutions (29) of the IEs (31)–(33), valid for the forward potential sweep, have been provided [34]. The coefficients are:

$$b_1 = 1 \tag{35}$$

and

$$b_{j+1} = \begin{cases} b_j\, \pi^{1/2} \frac{\lambda\delta^{1/2}(\lambda+j)^{-1/2} - (1-\delta) j^{1/2}}{(1-\delta) j - \lambda\delta} & \text{when } j \neq \lambda\delta(1-\delta)^{-1} \\ -b_j\, \pi^{1/2}(1+\delta)(2j^{1/2})^{-1} & \text{when } j = \lambda\delta(1-\delta)^{-1} \end{cases} \tag{36}$$

for $j = 1, 2, 3, \ldots$.

3 Computational details

Computational experiments were performed on a personal computer having an Intel Pentium D processor operating at 3 GHz, and a 2 GB operational memory. The numerical code was written in C++ using extended precision (long double variables having 80 bits and 18 digit precision, compliant with the IEEE 754 standard), and compiled as a 32-bit console application, using Borland C++ Builder 6.0 compiler. The code was run under MS Windows XP Professional.

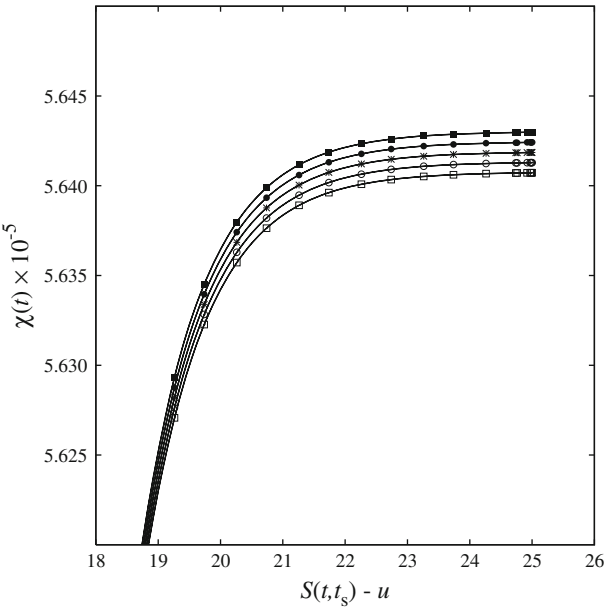

Fig. 6 Cyclic voltammetric current functions $\chi(t)$ obtained by the adaptive Huber method from Eqs. (31)–(33), assuming $u = 15$, $t_s = 40$, $\lambda = 10^{12}$, and $\delta = 0.9996$(*open square*); 0.9998(*open circle*); 1 (*asterisk*); 1.0002 (*filled circle*); and 1.0004 (*filled square*), in example 4. Method parameters are: $tol = 10^{-4}$, $h_{\text{start}} = 0.01$ and $h_{\max} = 1$. *Solid lines* represent analytical steady-state current functions given by Eq. (34). Initial parts of the voltammograms are not shown

4 Results and discussion

Figures 1–4 present typical plots of the adaptively simulated transients from examples 1–4, respectively. In every figure the adaptive results are compared to reference solutions obtained in an alternative way. Specifically, the reference solutions for example 1 result from the application of the DASSL integrator [42], implemented in the ELSIM 3.0 program [43], to the ODE system (10)–(13). Absolute error tolerance parameter value of 10^{-12} has been assumed in DASSL. The reference solutions for example 2 result from the analytical formula (26), and the reference solutions for examples 3 and 4 result from the finite-difference simulations using the Crank-Nicolson method [44] for partial differential equations, implemented in ELSIM [43]. As can be seen in Figs. 1–4, the results obtained by the adaptive Huber method match well the reference solutions. The automatic integration step selection is equally successful as it was in the case of previously considered kernels [11–17]. The adaptive algorithm concentrates grid nodes in the places of an increased variability of the IE solutions, such as the locations of voltammetric peaks in examples 1, 3 and 4, or initial rapid current variation in example 2.

When simulating diffusion to spherical electrodes, it is important to ensure that correct results are obtained even for extremely small electrode radii, which usually present a difficulty for simulations. We present relevant tests for example 3. By assuming that

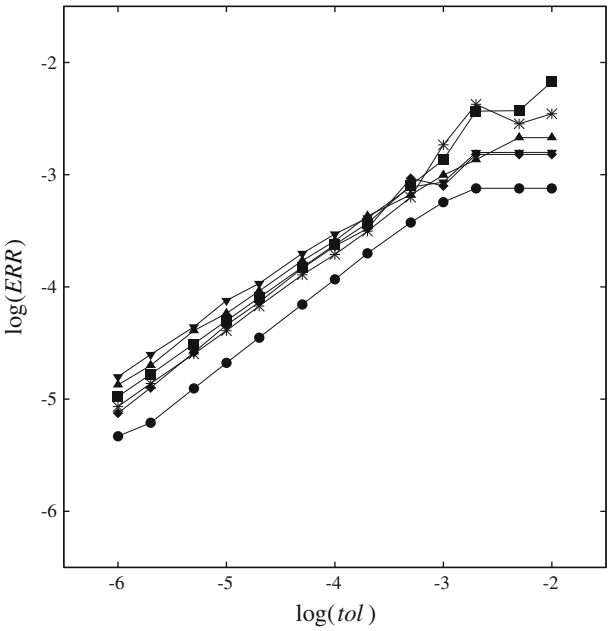

Fig. 7 Effect of the error tolerance parameter *tol* on the error measure *ERR* of the adaptive solutions of the IEs in examples 1–4. Notation: example 1, errors of $\psi_1(t)$ (*asterisk*); example 1, errors of $\psi_2(t)$(*square*); example 2, errors of $\psi(t)$ (*circle*); example 3, errors of $\chi(t)$(*triangle*); example 4, errors of $\chi(t)$ in the case of $\delta = 0.5$(*inverted triangle*); example 4, errors of $\chi(t)$ in the case of $\delta = 2$(*diamond*). Parameters other than *tol* are as in Figs. 1–4

the smallest radius of spherical (or formally equivalent hemi-spherical) electrodes is about 2 μm [45], and by taking the typical values of $D = 5 \times 10^{-10}\text{m}^2/\text{s}$, $T = 293\text{K}$, and $v \geq 0.01$ V/s, the highest physically reasonable ρ value in example 3 is about 20. Figure 5 shows that the adaptive Huber method has no difficulty with generating correct solutions, consistent with the steady-state formula (28), even for much greater ρ. Similarly, when simulating homogeneous reaction-diffusion problems, it is important to ensure that correct results are obtained for extremely large homogeneous reaction rate constants. Such large rate constants correspond to large coefficients λ, $\lambda(1-\delta)^{-1}$, $\lambda\delta(1-\delta)^{-1}$, $\lambda(\delta-1)^{-1}$, and $\lambda\delta(\delta-1)^{-1}$ in Eqs. (31) and (32) in example 4. By taking δ close to unity, the last four coefficients are additionally enlarged. Figure 6 reveals that the adaptive Huber method provides correct solutions, consistent with the steady-state solution (34), under such extreme conditions in example 4.

From the results shown in Figs. 5 and 6 we further deduce that the steady-state solutions (28) and (34) are easily computed with the same absolute error tolerance *tol* in a wide range of ρ or λ parameters, even though the absolute values of the current functions vary (with ρ or λ) over several orders of magnitude. The phenomenon of improving accuracy of simulations with increasing λ was observed in Ref. [15] for the kernel $K(t,\tau) = \exp[-\lambda(t-\tau)](t-\tau)^{-1/2}$; the IEs involving the present kernel cases B, D, E and F are seen to exhibit similar behaviour. The robustness of the

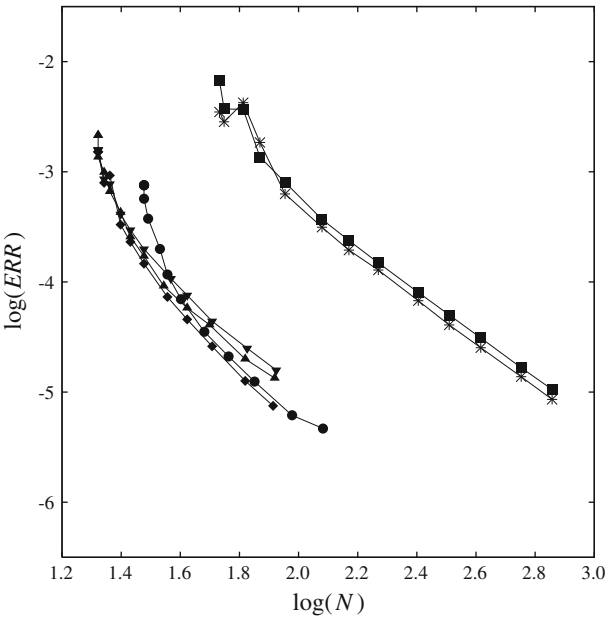

Fig. 8 Dependences of the error measure *ERR*, of the adaptive solutions of the IEs in examples 1–4, on the total number N of integration steps needed. Notation and parameters are as in Fig. 7. The successive data points (from left to right) correspond to $tol = 10^{-2}, 5 \times 10^{-3}, 2 \times 10^{-3}, 10^{-3}, 5 \times 10^{-4}, 2 \times 10^{-4}, 10^{-4}, 5 \times 10^{-5}, 2 \times 10^{-5}, 10^{-5}, 5 \times 10^{-6}, 2 \times 10^{-6}, 10^{-6}$

adaptive Huber method in this respect is secured by the analytical determination of the kernel-dependent method coefficients [18].

Convergence tests of the method have been performed in the way similar to that in Refs. [11–18], by observing how a selected error measure *ERR* varies with the error tolerance parameter *tol* of the method. In example 1 two *ERR* measures were defined as the absolute values of the differences between the forward peak heights of $\psi_1(t)$ and $\psi_2(t)$ obtained by the adaptive Huber method, and the respective reference peak height values obtained by DASSL: $\psi_1(10.13) = 0.25477647956$, and $\psi_2(15.67) = 0.24567784138$. In example 2 *ERR* was the largest absolute value of the difference between adaptively simulated $\psi(t)$, and the analytical predictions of Eq. (26). Finally, in examples 3 and 4 *ERR* was the largest absolute value of the difference between adaptively simulated $\chi(t)$ and the reference values of $\chi(t)$ obtained by the numerical summation of the series (29) in the common region of its practical summability, i.e. for $t \leq u$.

Figure 7 confirms the convergence, by showing that in all examples *ERR* decreases with decreasing *tol*. Ideally, *ERR* should be equal to *tol*, or at least proportional to *tol*. Figure 7 reveals some departure from ideality: *ERR* decreases slower with *tol*, than *tol* itself, reaching in the worst case (for the lowest *tol* values in Fig. 7) about $10 \times tol$. Similar results have been previously obtained [14–17] for the second kind Volterra IEs involving kernels $K(t,\tau) = 1$, $K(t,\tau) = (t-\tau)^{-1/2}$, and $K(t,\tau) =$

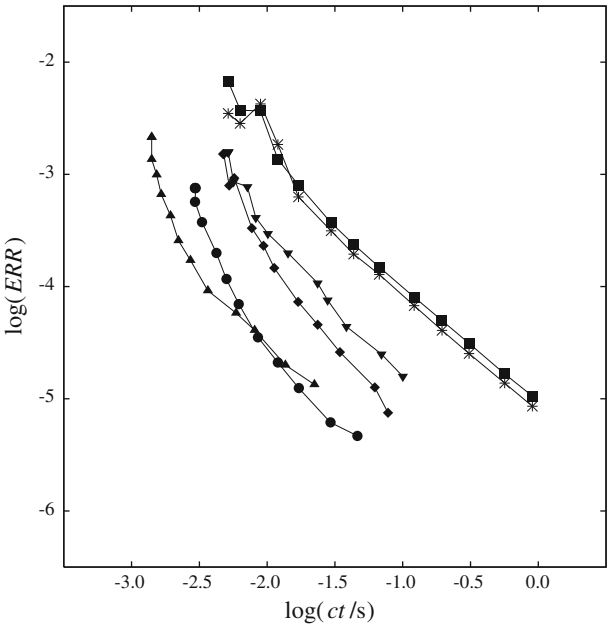

Fig. 9 Dependences of the error measure *ERR*, of the adaptive solutions of the IEs in examples 1–4, on the computational time (*ct*). The computational time values are averages over 500 identical runs of the program. Notation and parameters are as in Fig. 7, and parameter *tol* values are as given in Fig. 8

$\exp[-\lambda(t-\tau)](t-\tau)^{-1/2}$. As all the present examples are also second kind Volterra IEs, consistency with the previous findings can be stated.

From the slope of the dependences of $\log(ERR)$ on $\log(N)$, where N is the number of integration steps needed to accomplish simulation for a given *tol*, one can determine practical accuracy orders. Figure 8 reveals that these orders are close to 2, in an approximate agreement with the theoretical predictions for the present kernels (2) and (3), and in accord with all previously considered examples [11–18].

Finally, Fig. 9 presents efficiency plots of the adaptive simulations of examples 1–4. We see that the computations are rather fast. The longest computational times of about 1 second are observed in example 1, when the smallest $tol(=10^{-6})$ is chosen. This result is comprehensible, since the IE system in example 1 requires more computational effort than the single IEs in examples 2–4. The computational times are comparable to those previously observed for other examples [11–18].

5 Conclusions

Results obtained in this work confirm the validity of the adaptive Huber method, extended to kernels (2) and (3), for the simulations of controlled-potential electrochemical transients. The performance of the extended method is found similar to that previously observed for the IEs involving exclusively kernels $K(t,\tau)=1$, $K(t,\tau)=(t-\tau)^{-1/2}$, and $K(t,\tau)=\exp[-\lambda(t-\tau)](t-\tau)^{-1/2}$ with $\lambda>0$. The extended

method provides automatic solutions to the representative example IEs, without any prior knowledge of the temporal behaviour of the numerical solutions, but with an accuracy that can be effectively set up by choosing an appropriate value of the error tolerance parameter *tol*. In this way, well accurate and reliable solutions can now be obtained for a number of electrochemically important IEs not previously covered by the method.

References

1. L.K. Bieniasz, in *Modern Aspects of Electrochemistry*, vol. 35, ed. by B.E. Conway, R.E. White (Kluwer/Plenum, New York, 2002), p. 135
2. D. Britz, *Digital Simulation in Electrochemistry*, 3rd edn. (Springer, Berlin, 2005)
3. E. Gallopoulos, E. Houstis, J.R. Rice, Future Research Directions in Problem Solving Environments for Computational Science. Tech. Report CSD TR-92-032, Computer Sci. Dept., Purdue University, West Lafayette (1992)
4. E.N. Houstis, J.R. Rice, Math. Comput. Simul. **54**, 243 (2000)
5. A.J. Bard, L.R. Faulkner, *Electrochemical Methods, Fundamentals and Applications* (Wiley, New York, 1980)
6. A.M. Bond, M. Švestka, Collect Czech. Chem. Commun. **58**, 2769 (1993)
7. M. Trojanowicz, in *Modern Techniques in Electroanalysis*, ed. by P. Vanýsek (Wiley, New York, 1996), p. 187
8. T. Erichsen, S. Reiter, V. Ryabova, E.M. Bonsen, W. Schuhmann, W. Märkle, C. Tittel, G. Jung, B. Speiser, Rev. Sci. Instrum. **76**, 062204 (2005)
9. J. Mocak, in *Encyclopedia of Analytical Science*, ed. by P.J. Worsfold, A. Townshend, C.F. Poole (Elsevier, Oxford, 2005), p. 208
10. A. Huber, Monatsschr. Math. Phys. **47**, 240 (1939)
11. L.K. Bieniasz, Computing **83**, 25 (2008)
12. L.K. Bieniasz, Computing **83**, 163 (2008)
13. L.K. Bieniasz, Anal. Chem. **80**, 9659 (2008)
14. L.K. Bieniasz, Computing **87**, 35 (2010)
15. L.K. Bieniasz, Electrochim. Acta. **55**, 721 (2010)
16. L.K. Bieniasz, Appl. Math. Comput. **217**, 5622 (2011)
17. L.K. Bieniasz, J. Electroanal. Chem. **642**, 127 (2010)
18. L.K. Bieniasz, J. Comp. Meth. Sci. Eng., in press. doi:10.3233/JCM-2011-0391
19. V. Mirčeski, R. Gulaboski, J. Solid State Electrochem. **7**, 157 (2003)
20. R. Gulaboski, J. Solid State Electrochem. **13**, 1015 (2009)
21. K. Tokuda, N. Enomoto, H. Matsuda, N. Koizumi, J. Electroanal. Chem. **159**, 23 (1983)
22. J. Dutt, T. Singh, J. Electroanal. Chem. **182**, 259 (1985)
23. T. Singh, J. Dutt, S. Kaur, J. Electroanal. Chem. **304**, 17 (1991)
24. J.W. Weidner, P.S. Fedkiw, J. Electrochem. Soc. **138**, 2514 (1991)
25. J.W. Weidner, P.S. Fedkiw, J. Electrochem. Soc. **139**, 2076 (1992) (erratum)
26. J.R. Delmastro, D.E. Smith, J. Electroanal. Chem. **9**, 192 (1965)
27. J.R. Delmastro, D.E. Smith, Anal. Chem. **38**, 169 (1966)
28. M.L. Olmstead, R.S. Nicholson, J. Electroanal. Chem. **14**, 133 (1967)
29. A.M. Bond, R.J. O'Halloran, I. Ruzic, D.E. Smith, Anal. Chem. **48**, 872 (1976)
30. J. Goodisman, J. Electroanal.Chem. **144**, 33 (1983)
31. G. Diao, Z. Zhang, J. Electroanal. Chem. **410**, 155 (1996)
32. Š. Komorsky-Lovrić, M. Lovrić, J. Electroanal. Chem. **384**, 115 (1995)
33. L. Bieniasz, J. Electroanal. Chem. **170**, 77 (1984)
34. L.K. Bieniasz, J. Electroanal. Chem. **188**, 13 (1985)
35. J.R. Delmastro, G.L. Booman, Anal. Chem. **41**, 1409 (1969)
36. M. Lovrić, Y.I. Tur'yan, Croat. Chem. Acta. **76**, 189 (2003)
37. I. Shain, K.J. Martin, J.W. Ross, J. Phys. Chem. **65**, 259 (1961)
38. R.D. DeMars, I. Shain, J. Am. Chem. Soc. **81**, 2654 (1959)
39. R.S. Nicholson, I. Shain, Anal. Chem. **36**, 706 (1964)

40. L.K. Bieniasz, J. González, Á. Molina, E. Laborda, Electrochim. Acta. **56**, 543 (2010)
41. W.H. Reinmuth, Anal. Chem. **34**, 1446 (1962)
42. L.R. Petzold, in *Scientific Computing, Applications of Mathematics and Computing to the Physical Science*, ed. by R.S. Stepleman (North-Holland, Amsterdam, 1983), p. 65
43. L.K. Bieniasz, Comput. Chem. **21**, 1 (1997)
44. J. Crank, P. Nicolson, Proc. Cambridge Phil. Soc. **43**, 50 (1947)
45. A.M. Bond, Analyst **119**, R1 (1994)